atmosphere

MDPI

Article

Two-Stage Process for Understanding Summer Monsoon Impact on Ozone over Eastern China

Tianyu Zhu [1,*], Wei Dai [1], Yuhang Wang [2] and Mingjie Xie [1]

[1] Collaborative Innovation Center of Atmospheric Environment and Equipment Technology, Jiangsu Key Laboratory of Atmospheric Environment Monitoring and Pollution Control, School of Environmental Science and Engineering, Nanjing University of Information Science & Technology, Nanjing 210044, China; daiweideemail@nuist.edu.cn (W.D.); mingjie.xie@nuist.edu.cn (M.X.)

[2] School of Earth and Atmospheric Sciences, Georgia Institute of Technology, Atlanta, GA 30332, USA; yuhang.wang@eas.gatech.edu

* Correspondence: 20201212035@nuist.edu.cn

Abstract: The ozone levels over eastern China show a distinct two-stage process, with an inter-seasonal low (ISL) between May and September, unlike other polluted northern low-to-mid-latitude regions. The timing and progression of this low from southern to northern China align with the East Asian summer monsoon (EASM). The EASM leads to a decrease (ΔISL1) during the first stage and an increase (ΔISL2) during the second stage. The response varies by region, with the ΔISL1 (25 to 60 ppbv) greater than the ΔISL2 (20 to 30 ppbv) in the North China Plain (NCP), and the ΔISL1 (20 to 35 ppbv) less than the ΔISL2 (35 to 55 ppbv) in the Pearl River Delta (PRD). The ozone levels are inversely related to the monsoon index (MI) during stage 1 ($r = -0.69$, $p < 0.05$), while during stage 2, the ozone levels are anticorrelated with the maximum MI in the NCP and PRD ($r = -0.73$ and -0.80, $p < 0.05$). And the average ozone levels are anticorrelated with the MI during stage 2 in the Yangtze River Delta (YRD) ($r = -0.71$, $p < 0.05$). The simulations using CMIP6 suggest that intensified EASM caused by greenhouse emissions may help reduce summertime ozone pollution. The results show that different regions require different pollution control policies during pre- and post-monsoon seasons.

Keywords: ozone; summer monsoon; inter-seasonal low

Academic Editor: Kostas Eleftheratos

Received: 6 March 2025
Revised: 4 April 2025
Accepted: 9 April 2025
Published: 10 April 2025

Citation: Zhu, T.; Dai, W.; Wang, Y.; Xie, M. Two-Stage Process for Understanding Summer Monsoon Impact on Ozone over Eastern China. *Atmosphere* **2025**, *16*, 444. https://doi.org/10.3390/atmos16040444

1. Introduction

Surface ozone is harmful to humans and vegetation [1,2]. In China, surface ozone pollution during the warm season is severe, with frequent high-ozone events [3,4]. Meteorological conditions can significantly affect surface ozone concentrations [5]. The most prominent large-scale circulation feature in the summer over eastern China is the East Asian summer monsoon (EASM) [6,7]. Surface observations and model simulations have shown that surface concentrations of ozone and other pollutants tend to decrease under the impact of the EASM, which is due to an unfavorable photochemical environment, precipitation, and the transport of clean oceanic air masses from the tropical Pacific Ocean [8–11].

A notable feature of the EASM onset over eastern China is the formation of the Meiyu rain band in early summer, predominantly affecting the southern region [12–14]. As the EASM progresses northward and northeastward, the western Pacific subtropical high, a dominant atmospheric high-pressure system that typically forms over the northwestern Pacific Ocean in the summer, extends over the southern region by midsummer. By late summer, the EASM begins to dissipate in the northern region and subsequently retreats southward.

The interannual variability in the EASM is reflected in the precipitation variation: a stronger EASM corresponds with more rainfall over northern China, whereas a weaker EASM leads to more rainfall over the Yangtze–Huai River Basin [15], a region to the south of the North China Plain (NCP) region extending into the Yangtze River Delta (YRD) region, shown in Figure 1. It contributes to the interannual variability in the surface ozone. Li et al. [16] found that the surface ozone in eastern China between 28° N and 42° N is reduced when the EASM is strong.

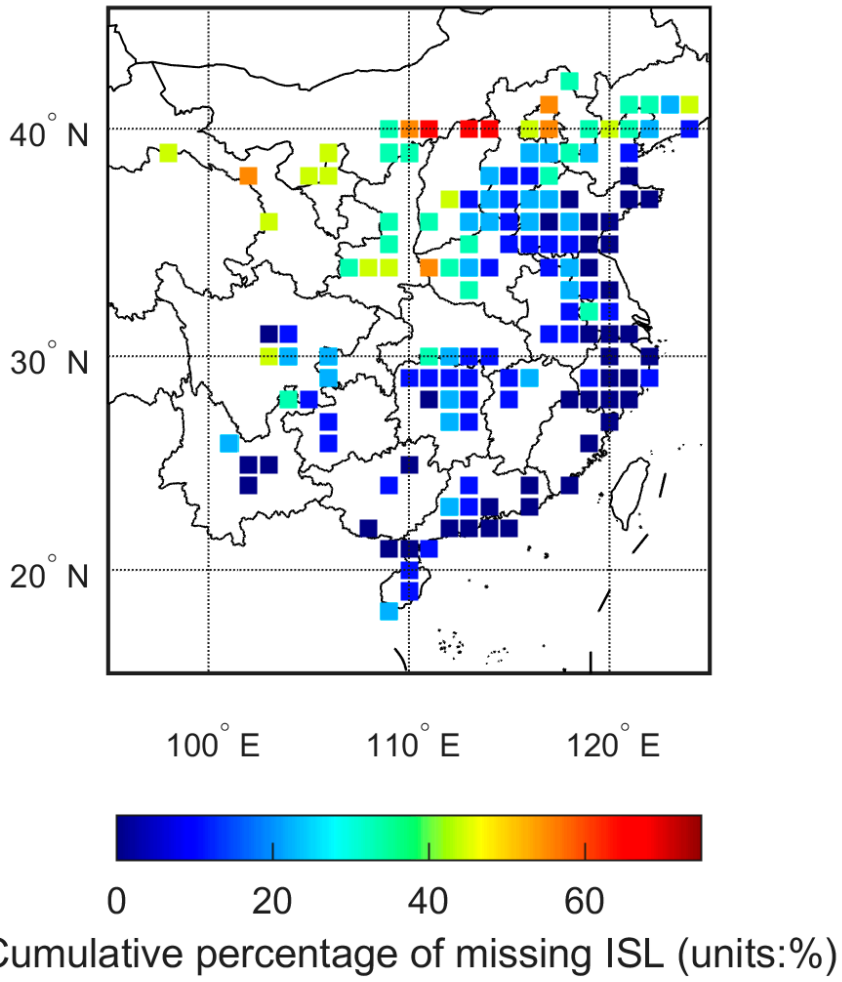

Figure 1. Percentage fraction of site-years between 2014 and 2022 during which no ISL was identified. The data are presented on a 1°x1° grid. For each grid cell, the fraction is calculated by dividing the total number of site-years without ISLs by the total number of site-years within that cell.

Vingarzan [17] reviewed the historical background surface ozone data for Canada and the United States and found that the annual ozone cycle is characterized by a spring–early summer maximum, peaking during May. In contrast, the background ozone over eastern China shows very different seasonal variations due to the EASM. Tanimoto et al. [18] analyzed the surface ozone seasonality data from the Acid Deposition Monitoring Network and found a spring maximum and a summer minimum at all seven remote stations, with differences of 20–35 ppbv. He et al. [19] noted the pre- and post-monsoon peaks, with a summer trough at three mountain monitoring sites in eastern China. The variations between the two peaks and the trough were in the range of 30 to 40 ppbv.

The difference in the summertime surface ozone variation is just as large over polluted sites. Oltman and Levy [20] found summer ozone peaks over the polluted eastern United States due to anthropogenic emissions. In contrast, the inter-seasonal low (ISL) of the

surface ozone over polluted eastern China sites between May and September has been reported in many studies [21–23]. However, previous studies have mainly focused on the impact of the EASM on the summer average of ozone concentrations. In this study, we examine the processes by which the EASM affects the surface ozone over eastern China using a two-stage framework. We use this framework to calculate different variations in the ISL and examine its correlation with the EASM during each stage. The regional characteristics are examined in Section 3.1. The effect of the EASM on the interannual variation in ozone is discussed in Section 3.2, including the interannual variations and correlations in Sections 3.2.1 and 3.2.2, respectively. In Section 3.3, we also evaluate the potential changes in the EASM's impact on ozone due to climate change, using Coupled Model Intercomparison Project Phase 6 (CMIP6) simulations. The possible application of this framework is discussed in Section 4. This study aims to quantify the EASM's impact on the ozone over different regions under a two-stage framework, incorporating both observational characteristics and potential climate change effects. Notably, the ISL over eastern China is quantitatively calculated, and serves as the boundary demarcating the two stages in the framework. The different correlations in the results could contribute to pollution control policies that consider the differences during each stage and in different regions.

2. Materials and Methods

2.1. Observation and Model Simulation Data

Surface ozone observation data from 2014 to 2022 were obtained from the China National Environmental Monitoring Centre (CNEMC). To ensure the representativeness of data used in this study, 710 sites were selected based on data record continuity. The selected sites have at least half a month of valid data each month from 2014 to 2022.

Monthly meteorological data were obtained from ERA5 dataset of the European Centre for Medium-Range Weather Forecasts (ECMWF) from 2014 to 2022 [24], which are used for monsoon index (MI) calculation. In addition, wind fields at different pressure levels are examined. Climate projections produced by Coupled Model Intercomparison Project Phase 6 (CMIP6) models are used to investigate the possible monsoon impact on ozone under a changing climate. CMIP6 models provide multi-model climate projections based on alternative scenarios that are directly relevant to societal concerns. These datasets are calculated under a shared socio-economic pathway (SSP) framework. In this study, potential monsoon variations are compared for the "sustainability" scenario SSP126 and the "fossil-fueled development" scenario SSP585 to highlight the most significant differences. SSP126, with an anthropogenic radiative forcing level of 2.6 W/m² by 2100, approximately corresponds to the optimistic scenario of Representative Concentration Pathway (RCP) 2.6 of CMIP5, which is compatible with the 2 °C warming target. SSP585, with a radiative forcing of 8.5 W/m² by 2100, represents the upper end of the SSP spectrum [25,26].

Eleven CMIP6 models with close configurations were selected. Monthly atmospheric data from CMIP6 are used for estimating monsoon intensity from 2015 to 2099, with the table ID "Amon". For consistency, all datasets for eleven CMIP6 models have the same variant label "r1i1p1f1", removing the possible impact of method configurations on realization (r), initialization (i), physics (p), and forcing (f). Grid labels are all set to "gn", meaning that model data are reported on a native grid. Nominal resolutions of all models are 100 km. Variables "ua" and "va", representing the eastward and northward winds, respectively, are used for monthly MI calculations. The information for these models is listed in Table 1.

Table 1. Eleven CMIP6 model simulations used in this study.

Model	Institution	Domain Grid Dimension (Longitude × Latitude)
AWI-CM1.1-MR	AWI/Germany	384 × 192
BCC-CSM2-MR	BCC/China	320 × 160
CAMS-CSM1.0	CAMS/China	320 × 160
CAS-ESM2.0	CAS/China	256 × 128
CESM2-WACCM	NCAR/USA	288 × 192
CMCC-CM2-SR5	CMCC/Italy	288 × 192
CMCC-ESM2	CMCC/Italy	288 × 192
MPI-ESM1.2-HR	DKRZ/Germany	384 × 192
MRI-ESM2.0	MRI/Japan	320 × 160
NorESM2-MM	NCC/Norway	288 × 192
TaiESM1	AS-RCEC/China	288 × 192

2.2. ISL Calculation

In this study, ISL is defined as the process of decline and recovery of ozone levels from May to September. The occurrence of ISL leads to a clear valley during summer, with two peaks before and after. To compute the ISL, we first regress the observation data with monthly-to-seasonal periodic functions. Parrish et al. [27] used the first two Fourier transform terms, yearly and semi-yearly harmonics, to fit ozone data and compute the seasonal cycle. We use a more extensive Fourier transform expansion to track monthly-to-seasonal cycles and calculate the ISL:

$$(\mathrm{t}) = \overline{y} + \sum_{i=1}^{n} A_i \cos[2\pi f_i (t - \varphi_i)] \quad (1)$$

where $\overline{y}$ represents the concentration of pollutants, e.g., daily maximum 8 h average (MDA8) ozone; $\overline{y}$ is the annual mean value of a year; n is the total number of harmonics; and A_i, f_i, and φ_i are the amplitude, frequency, and phase of harmonics i, respectively. For yearly data, there are a total of 12 harmonics with a periodicity longer than 1 month (i.e., n = 12), which are included to calculate the monthly ISL values. We use the Lomb–Scargle method to compute the least-square regression in Equation (1), a well-known technique to compute periodicity of unequally spaced data, which is particularly helpful for observation data from the early years [28–30].

After regressing the daily MDA8 ozone data using Equation (1), the summer (June–August) minimum is determined first (e.g., the ISL). Then, the maximum before and after the minimum, from May to September, is determined. The differences in the first and second maximum from the summer minimum are calculated as ΔISL1 and ΔISL2, respectively. Not all sites are affected by EASM. Figure 1 shows the fraction of site-years during which no ISL was identified. The northern and northwestern regions are the least influenced by EASM, while the inland regions are less affected compared to coastal areas, where moisture supply is more abundant.

2.3. Monsoon Index

To quantify monsoon activity, an appropriate monsoon index (MI) is essential. There are several different indices for the East Asian summer monsoon (EASM). Li and Zeng [31] defined a dynamical normalized seasonality (DNS) index, which has been widely used to represent the activity of EASM [32,33]. It is positive during summer and negative during other periods, with a significant peak in August. The onset and developing process of EASM is directly reflected by the increase in DNS index (from May to August), and the retreat process of EASM is reflected by the decrease in DNS index (from August to

September or October). The DNS index has a large positive correlation with convective activity over the vicinity of the Philippines and the warm pool region of the western Pacific. However, the negative correlation between DNS index and rainfall over the Yangtze River Basin suggests that DNS index is not appropriate for our study.

Zhao et al. [34] found that the 200 hPa zonal wind anomalies in the southern (~5° N), middle (~20° N), and northern bands (~35° N) of East Asia correspond to the most significant empirical orthogonal function (EOF) tripolar pattern associated with EASM variations. They defined an EASM index based on the zonal wind anomalies, and showed that this index captures well the seasonal shift in the Meiyu–Baiu rain belt well, and its changes represent anomalous climate patterns in early and late summer. It considers both the precipitation pattern at low levels and the circulation mode in the upper levels and thus represents more details of local circulation than the DNS index, which is beneficial to this study. When MI is above average, precipitation anomalies display a zonally elongated distribution: suppressed rainfall over the South China Sea extending eastward, and increased rainfall extending from the Yangtze River Basin crossing the Korean Peninsula to Japan. This feature effectively separates the monsoon activity in the Yangtze River Delta from Pearl River Delta region. We use it as the monsoon index (MI) and it is calculated as follows:

$$\begin{aligned} \mathrm{MI} = \mathrm{Nor}[&\mathrm{u}(105^\circ\ \mathrm{E}\text{–}140^\circ,\ 2.5^\circ\text{–}10^\circ\ \mathrm{N}) \\ &- \mathrm{u}(105^\circ\text{–}140^\circ\ \mathrm{E},\ 17.5^\circ\text{–}22.5^\circ\ \mathrm{N}) \\ &+ \mathrm{u}(105^\circ\text{–}140^\circ\ \mathrm{E},\ 30^\circ\text{–}37.5^\circ\ \mathrm{N})] \end{aligned} \quad (2)$$

where Nor denotes the normalization of zonal mean wind at 200 hPa. We apply Equation (2) to monthly mean zonal wind speed to compute monthly MI from May to September. A high MI represents a stronger EASM, and its variation implies a change in EASM intensity.

3. Results

3.1. Regional Characteristics of EASM's Two-Stage Effects on Ozone

Figure 2a shows an illustration of the ISL for a site in Shanghai. The progression of the EASM is reflected in the timing of the ozone ISL valley (Figure 2b). The ISL valley occurs mainly in late June to early July over southern China, and in late July to early August over northern China. It is noteworthy that the geographic separation of the ISL valley timing is around the Huai River (~3° N), which has traditionally been used to separate northern and southern China for climatic and cultural reasons. The broad regional homogeneity in Figure 2b is consistent with previous studies of the ozone at remote mountain sites. Wang et al. [35] conducted five-year continuous ozone measurements at the summit of the Nanling Mountains (112.8° E, 24.6° N) in southern China, and found a summer minimum in July. He et al. [19] carried out continuous ozone observations and found the minimum in August at Mount Hua (110.0° E, 34.4° N).

We computed the ΔISL1 and ΔISL2 as the decrease and increase in the ozone from the ISL in stages 1 and 2, respectively. Figure 2c,d show their distributions. Over eastern China, the ozone reductions induced by the EASM are in the range of 20–60 ppbv, which are highly important for modulating ozone concentrations during the summer season. Without the EASM modulation, the summertime ozone over eastern China would have been much higher given the same emissions of ozone precursors.

Over the NCP region, the ΔISL1 values, ranging from 25 to 60 ppbv, are higher than the ΔISL2, ranging from 20 to 30 ppbv. The difference reflects the significant ozone production and increases prior to the arrival of the EASM in the region. It is consistent with previous studies that have found high ozone concentrations in the NCP region in June and July [36]. During the monsoon period, suppressed photochemical production, enhanced wet scavenging, and the transport of marine air masses lead to the ISL [8–11,21,22]. After

the EASM's impact dissipates in August, the decrease in solar radiation from late summer to fall leads to a recovery of ozone concentrations that are below the level reached during the pre-monsoon season.

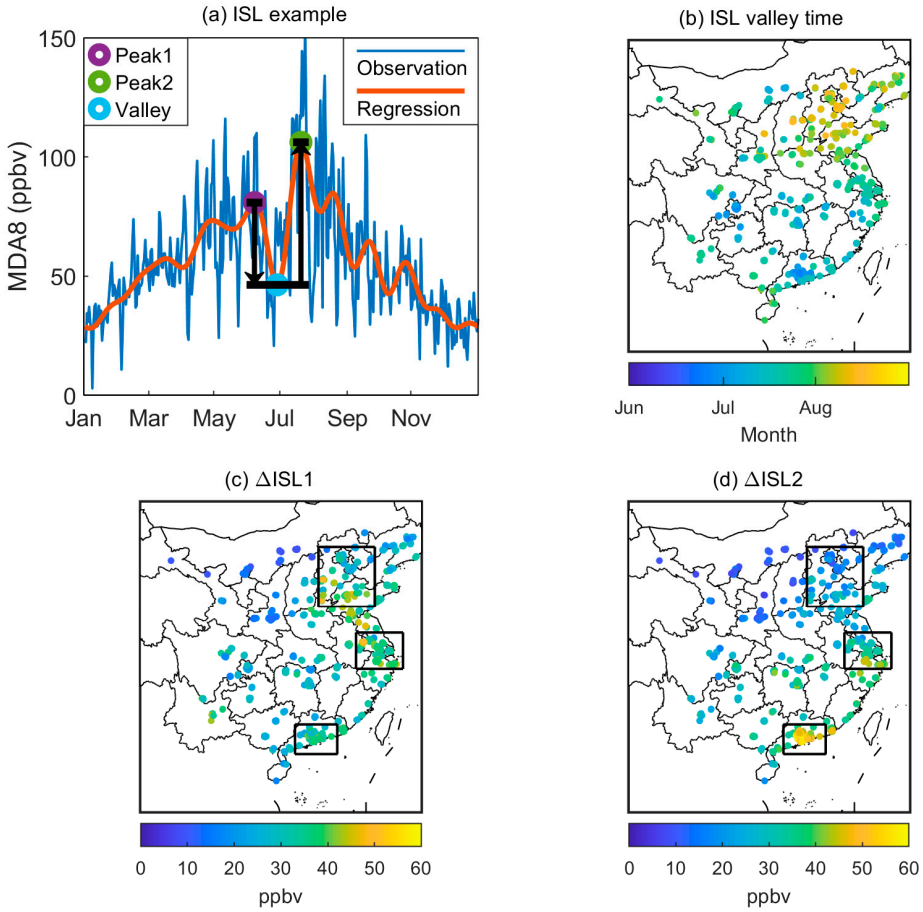

Figure 2. Ozone ISLs in eastern China during 2014–2022: ISL example (**a**), distribution of ISL valley time (**b**), distribution of ΔISL1 (**c**), and ΔISL2 (**d**). ISL example (**a**) shows observed daily MDA8 ozone concentrations at a site (121.47° E, 31.30° N) in Shanghai for 2017. The Equation (1) regression line is shown in red. The blue dot denotes the summer minimum (ISL valley). The maximums before and after the summer minimum are denoted as peak 1 and peak 2, respectively. Their differences from the minimum are calculated as ΔISL1 and ΔISL2, respectively. The distributions of ISL valley (**b**), ΔISL1 (**c**), and ΔISL2 (**d**) are shown for regional comparison. The three black rectangles in (**c**) and (**d**) denote the NCP (114.0° E–120.0° E, 35.5° N–41.0° N), YRD (118.0° E–123.0° E, 29.5° N–33.0° N), and PRD regions (111.5° E–116.0° E, 21.0° N–24.0° N), respectively.

The magnitudes of the ΔISL1 and ΔISL2 are comparable, at 30–60 ppbv in the YRD region. The earlier onset of the EASM in the YRD than the NCP region leads to a lower pre-monsoon peak and longer stage 2 duration than in the NCP region (Figure 2), both of which contribute to more comparable ΔISL1 and ΔISL2 levels. The rainy Meiyu season is a manifestation of the EASM, accounting for about half of the summer precipitation [14,37]. It generally commences in early to mid-June and ends in mid-July, and causes unfavorable meteorological conditions for ozone production, such as reduced solar radiation and significant precipitation [38,39]. The timing of the ISLs in the YRD region aligns closely with the end of the Meiyu season, suggesting that the ΔISL1 is caused by the cumulative effect of the Meiyu and the ΔISL2 is due to ozone recovery after the Meiyu. As a result, the relative humidity is a significant indicator of the ozone level in the YRD region [40].

The asymmetry in the ΔISL1 and ΔISL2 in the Pearl River Delta (PRD) region is opposite to that in the NCP; the magnitude of the ΔISL2 (35 to 55 ppbv) is 50% to 100% higher than the ΔISL1 (20 to 35 ppbv). The phase difference between the NCP and PRD reflects, in part, the difference in latitudinally dependent solar insolation, which enhances photochemical ozone production and is conducive for the formation of stagnant high-pressure systems. After the monsoon minimum, the solar intensity decreases much more rapidly in the NCP than in the PRD region, hindering the photochemical production of ozone [41]. In comparison, the solar insolation decline in the PRD region is more moderate. Furthermore, the period after the monsoon ozone minimum is longer in the PRD than in the NCP region, contributing to a higher ΔISL2 in the PRD region.

3.2. Effect of the EASM on the Interannual Variation in Ozone

3.2.1. Interannual Variations in MI and Ozone

The two-stage processes over eastern China due to the EASM dominates the variations in summertime ozone. The EASM exhibits considerable year-to-year variability [15,42], which in turn influences the interannual variation in ozone levels in the region. This relationship between the EASM dynamics and ozone concentrations underscores the complex interplay between meteorological patterns and air quality in eastern China. The monthly MI index (Equation (2)) is the metric we use in this analysis, where a high MI represents a stronger EASM. To improve the EASM characterization, we extend the analysis from summer (June–August, JJA) to May and September (e.g., Figure 2a). We define stage 1 as the period from May 1 to the date of the ISL (Figure 2b), and stage 2 as the period from the ISL to the end of September.

We examine how the average MDA8 ozone concentrations, including the summer average (ozone (JJA)), stage 1 average (ozone (S1)), and stage 2 average (ozone (S2)), relate to the MI summer average (MI (JJA)), maximum (MI (Max)), minimum (MI (Min)), stage 1 (MI (S1)), and stage 2 (MI (S2)) (Figure 2 and Table 1). The MI (Max) and MI (Min) are computed for May through September. Changing the period to JJA does not change the results. Given the definition of the MI (Equation (2)), the interannual variations in the MI (JJA), MI (Max), and MI (Min) are the same for the three regions (Figure 3), but those for MI (S1) and MI (S2) are slightly different due to the difference in the periods of stages 1 and 2 among the three regions (Figure 2b).

The left panels in Figure 3 show that the regional difference between ozone (S1) and ozone (S2) is large. Over the NCP region, ozone (S1) is comparable to ozone (JJA),both displaying parabolic curves with maximums around 2019. Ozone (S2), on the other hand, is about 10 ppbv lower, with a maximum difference of ~20 ppbv in 2018. These general characteristics are consistent with the ΔISL1 and ΔISL2 in Figure 2, showing a relatively small post-monsoon ozone recovery. The opposite is found over the PRD region. Ozone (S2) is higher than ozone (S1) by 5–10 ppbv generally. The difference between ozone (S1) and ozone (S2) is complex over the YRD region. Ozone (S1) is higher than ozone (S2) in 2014 and 2017–2019 by 10 ppbv, similar to northern China. In other years, ozone (S1) and ozone (S2) are comparable in most cases, except in 2016, when ozone (S2) is higher by nearly 10 ppbv. This complexity in the differences between ozone (S1) and ozone (S2) is due in part to a higher ΔISL1 in the northern YRD, but a higher ΔISL2 in the southern YRD (Figure 2). Furthermore, the double-peak feature between 2016 and 2020 and the subsequent increase from 2021 to 2022 are found in both ozone (S1) over the YRD region and ozone (S2) over the NCP region, reflecting the post-Meiyu south-to-north progression of the EASM and the significant role of the EASM in regulating the summertime ozone over eastern China.

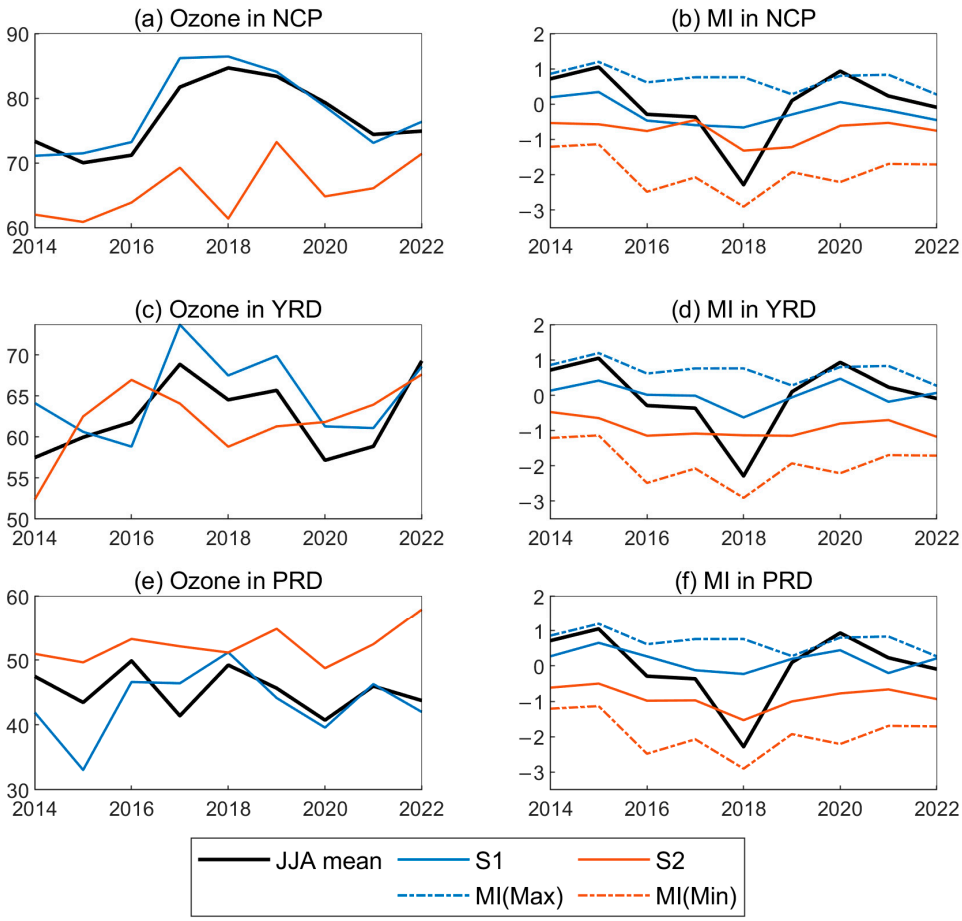

Figure 3. Interannual variations in the ozone concentrations (left column) and MIs (right column) for the NCP, YRD, and PRD regions from 2014 to 2022. Yearly averages for the summer (June−August, JJA, solid black lines), stage 1 (solid blue lines), and stage 2 (solid red lines) are shown for the ozone (ppbv) and MIs (unitless). Also shown are the yearly maximum (dashed blue lines) and minimum MI (dashed red lines) values for May–September. These variables imply different variations in the ozone and EASM during different periods.

3.2.2. Correlations Between MI and Ozone

Table 2 shows that the summertime ozone is anticorrelated with the MI, as expected. Although the correlation coefficients between the ozone (JJA) and MI (JJA) are ≤ -0.5 for all three regions, they are not statistically significant, partly because of the limited size of the dataset. A less apparent reason is the occasional prevalence of other meteorological effects that limit the ability of the EASM to modulate ozone concentrations, such as occurred in 2018. Chen et al. [43] found a strong Mongolian anticyclone and a weak extension of a western Pacific subtropical high in the summer of 2018, which contributed to anomalous northeasterlies over eastern and southern China at 850 hPa (Figure 4), and an anomalous easterly jet stream at 200 hPa (Figure 5), resulting in a minimum MI (JJA). Despite a much lower MI (JJA) in 2018 than in the other years, the ozone (JJA) concentrations in 2018 were not much higher, and were even lower than their values in 2017 or 2019 in the three regions. In comparison, the interannual variability in the MI (Max), MI (min), MI (S1), and MI (S2) was much smaller in 2018 compared to 2017 and 2019, and may explain the monsoon's effect on the ozone better.

Table 2. Correlations between monsoon index and ozone concentrations in different regions and periods.

Monsoon Index	NCP			YRD			PRD		
	Ozone (JJA)	Ozone (S1)	Ozone (S2)	Ozone (JJA)	Ozone (S1)	Ozone (S2)	Ozone (JJA)	Ozone (S1)	Ozone (S2)
MI (JJA)	−0.57	−0.64 *	0.13	−0.50	−0.39	0.03	−0.58	**−0.83** **	−0.18
MI (Max)	−0.25	−0.28	**−0.73** **	−0.57	−0.46	−0.07	−0.35	−0.34	**−0.80** **
MI (Min)	−0.57	−0.63	0.17	−0.23	−0.11	−0.12	−0.41	**−0.73** **	0.12
MI (S1)	−0.54	**−0.69** **	−0.26	−0.41	−0.36	0.10	−0.36	**−0.85** **	−0.06
MI (S2)	−0.52	−0.47	−0.08	**−0.71** **	−0.46	−0.34	−0.51	**−0.75** **	−0.19

* p-value is <0.10. ** p-value is <0.05. Significant correlations with p less than 0.05 are in bold fonts.

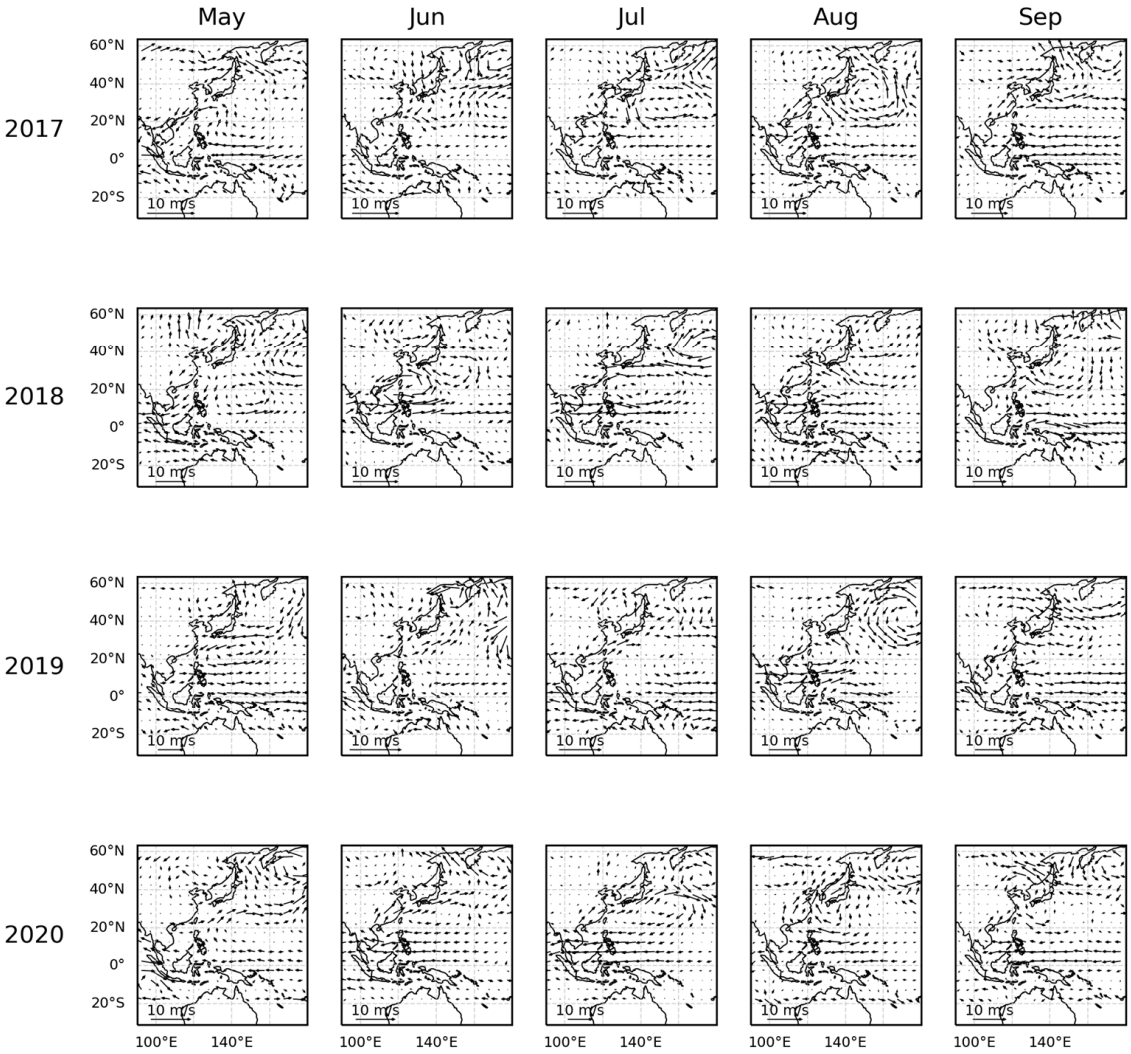

Figure 4. Anomalous 850 hPa wind fields from May to September during 2017–2020. Monthly anomalous wind fields are shown from May to September (left to right) for 2017 to 2020 (top to bottom). The deviations from the averages of 2014–2022 are shown.

Ozone (S1) is significantly anticorrelated with MI (S1) ($r = -0.69$, $p < 0.05$) in the NCP region. Since ozone (S1) and ozone (JJA) are closely related (Figure 3), ozone (JJA) is also anticorrelated with MI (S1) ($r = -0.64$, $p < 0.10$), reflecting the predominant influence of the stage 1 ozone on the average summertime ozone variations over the NCP, since the ΔISL1 is much higher than the ΔISL2 (Figure 2). Ozone (S2), on the other hand, is anticorrelated with MI (Max) ($r = -0.73$, $p < 0.05$). A similar result is found for the PRD region, where the asymmetric ozone response to the EASM is in a phase opposite to that of the NCP. Ozone

(S1) is most strongly anticorrelated with MI (S1) ($r = -0.85$, $p < 0.05$). It is also significantly anticorrelated with MI (JJA), MI (S2), and MI (Min). The strong correlations between ozone (S1) and these additional indices indicate a longer monsoon-affected period in the PRD region compared to the NCP region (Figure 2). Ozone (S2) is anticorrelated with MI (Max), as in the NCP region ($r = -0.80$, $p < 0.05$), indicating the effect of the maximum intensity of the EASM on the post-monsoon recovery of ozone in these regions.

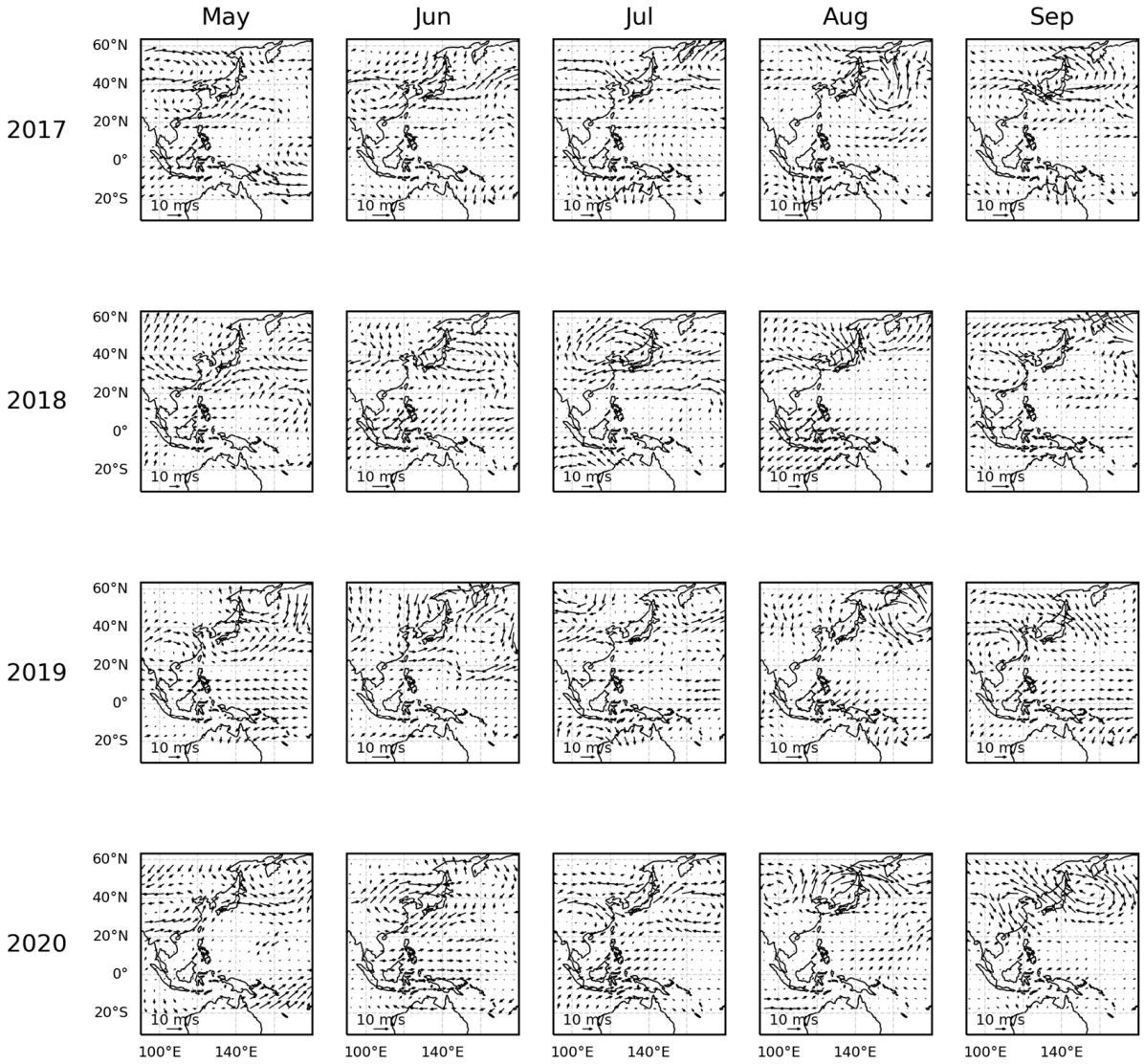

Figure 5. Same as in Figure 4, but for 200 hPa anomalous wind fields.

In the YRD region, however, only the anticorrelation between ozone (JJA) and MI (S2) is statically significant ($r = -0.71$, $p < 0.05$). The complex relationship between ozone (S1) and ozone (S2), and the comparable ΔISL1 and ΔISL2 (Figure 2), make the region's ozone variation challenging to explain with the MI indices. Unlike the NCP or PRD regions, the semi-stationary Meiyu process over the YRD region is unique and its timing and duration are not captured well by the monthly MI index (Equation (2)) we use in this study. A better temporally resolved MI will likely be necessary to represent the effect of the Meiyu on ozone concentrations. It may explain why MI (S2) correlates well with the YRD summertime ozone, since the monsoon process is not stationary during stage 2.

3.3. Effect of Climate Change on EASM

The analysis in the previous section shows that the negative effect of the EASM on summertime ozone concentrations over eastern China can be better analyzed using a two-stage process. Before this new understanding can be applied to study the effects of climate change on the EASM and the consequences for the ozone, the capability of climate models to simulate the two-stage process needs to be evaluated with observations (e.g., Figures 2 and 3; Table 2). In this work, we investigate only how climate change may affect the MI in summer.

We analyze the climate projections of 11 CMIP6 models (Table 1) by comparing the change in the summertime MI from the first 10 years (2015–2024) to the last 10 years (2090–2099) under the SSP126 and SSP585 scenarios. SSP585 represents a much warmer climate than SSP126 due to anthropogenic emissions [25]. Under the SSP126 scenario, the simulated MI change varies from −0.5 to 0.2, which is fairly significant (Figure 6). Despite the model spread, almost all the models predict a higher MI under the SSP585 scenario. The only exception is the CMCC-CM2-SR5 model, which predicts a lower MI in a warmer climate, possibly due to its weaker prediction of seasonal precipitation associated with monsoons over Asia [44]. A paired-sample t-test using MATLAB R2019b gives a value of $p < 0.01$. This result implies that anthropogenic emissions in the coming years will tend to increase the MI, which is associated in part with the extension of the rainy season driven by thermodynamics [45]. It will help to mitigate summertime ozone pollution over eastern China.

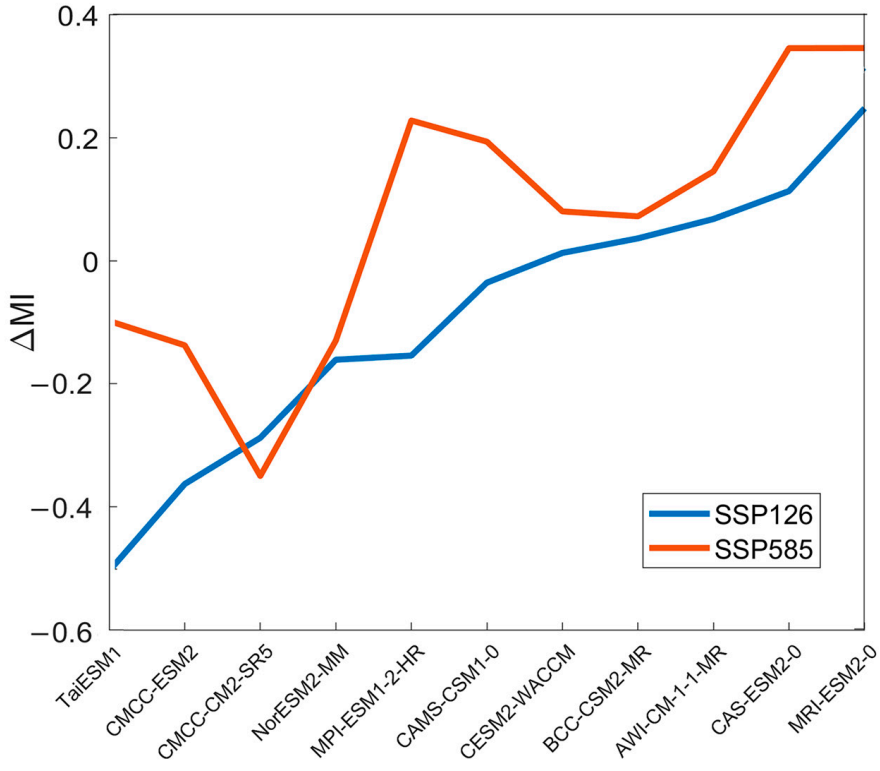

Figure 6. Change in decadal average summertime MI from 2015 to 2024 and 2090 to 2099 under SSP126 (blue) and SSP585 (red) scenarios simulated by 11 CMIP6 models.

4. Conclusions

The analysis of ozone and meteorological data from 2014 to 2022 reveals the significant impact of the East Asian summer monsoon (EASM) on summertime ozone levels over eastern China. The timing of the ozone ISL reflects the northward progression of the EASM during stage 1, when ozone levels decrease from early summer to the ISL. Stage 2 begins

with the dissipation of the EASM, leading to ozone increases from the ISL. The ozone response is highly asymmetric, with a strong decrease over the NCP region, where the ΔISL1 (25 to 60 ppbv) is greater than the ΔISL2 (20 to 30 ppbv). And there is a strong increase over the PRD region, where the ΔISL1 (20 to 35 ppbv) is smaller than the ΔISL2 (35 to 55 ppbv). The northern YRD region shows a response similar to that of the NCP region, while the southern YRD region aligns more with the PRD region, resulting in a more symmetric regional averaged response.

Framing the impact of the EASM on regional ozone levels with this two-stage process helps to clarify its effects on the observed interannual summertime ozone variations. In the NCP and PRD regions, ozone levels are anticorrelated with MI during stage 1 ($r = -0.69$ and -0.85, $p < 0.05$), while stage 2 ozone levels are anticorrelated with the maximum MI ($r = -0.73$ and -0.80, $p < 0.05$). In the YRD region, the summertime ozone is anticorrelated with the average MI during stage 2 ($r = -0.71$, $p < 0.05$), likely reflecting the unique semi-stationary nature of the Meiyu in this area, underscoring the complexity of monsoon circulation and its impact on air quality.

The CMIP6 projected decadal average changes in the MI from 2015 to 2024 and 2090 to 2099 show significant variability among the 11 models, with a large uncertainty spread. Additionally, the capability of climate models to simulate the two-stage process needs to be evaluated with observations. However, almost all the models predict positive MI changes under the SSP585 scenario rather than the SSP126, indicating that anthropogenic greenhouse gas emissions will tend to intensify the EASM, potentially mitigating summertime ozone pollution over eastern China in a changing climate.

In this study, we apply a two-stage framework to analyze the impact of the EASM on the summertime ozone over East China using both observational data and the CMIP6 projections. This two-stage process also has significant implications for mitigation strategies. For instance, ozone emission mitigation efforts should prioritize controlling the pre-monsoon ozone increase in the NCP region and the post-monsoon recovery in the PRD region. In the YRD region, the EASM during stage 2 has a greater influence on summer ozone levels, so the control policies will need to give more consideration to the meteorological factors in stage 2. Furthermore, the interactions among emissions, photochemistry, and meteorological processes need to be investigated separately for each stage.

There are still some uncertainties in this study that need further investigation. First, the definition of the ISL and MI would be improved by additional research. Second, the correlation analysis is limited due to the number of years analyzed. More continuous data are needed to examine the relationship between the ISL and EASM in the future. In addition, there are great uncertainties among the CMIP6 models, and their performance simulating the EASM's activity requires more evaluation. Further research is needed to determine the effectiveness of the link between the ISL and EASM in the face of climate change, as demonstrated by our study's findings.

Author Contributions: Conceptualization, T.Z. and Y.W.; methodology, T.Z.; software, T.Z. and Y.W.; validation, T.Z., Y.W. and M.X.; formal analysis, T.Z.; investigation, T.Z., Y.W. and M.X.; resources, Y.W.; data curation, Y.W.; writing—original draft preparation, T.Z.; writing—review and editing, T.Z., W.D., Y.W. and M.X.; visualization, T.Z.; supervision, Y.W. and M.X.; project administration, Y.W. and M.X.; funding acquisition, M.X. All authors have read and agreed to the published version of the manuscript.

Funding: This work was supported by the National Natural Science Foundation of China (42177211).

Institutional Review Board Statement: Not applicable.

Informed Consent Statement: Not applicable.

Data Availability Statement: The ERA5 data are available at https://cds.climate.copernicus.eu/datasets/reanalysis-era5-single-levels-monthly-means?tab=overview (single levels, last accessed on 15 January 2025) and https://cds.climate.copernicus.eu/datasets/reanalysis-era5-pressure-levels-monthly-means?tab=overview (pressure levels, last accessed on 15 January 2025). The CMIP6 data are available at https://esgf-ui.ceda.ac.uk/cog/search/cmip6-ceda/ (last accessed on 15 January 2025). The ozone observation data in this study were collected from the China National Environmental Monitoring Center (https://air.cnemc.cn:18007/, last accessed on 1 March 2023) and were uploaded from Zenodo via https://doi.org/10.5281/zenodo.14969783.

Acknowledgments: We thank the China National Environmental Monitoring Centre for providing the observation data, the European Centre for Medium-Range Weather Forecasts and the Climate Data Store for the ERA5 data, and the Earth System Grid Federation node for the CMIP6 data.

Conflicts of Interest: The authors declare no conflicts of interest.

References

1. Holm, S.M.; Balmes, J.R. Systematic Review of Ozone Effects on Human Lung Function, 2013 Through 2020. *CHEST* **2022**, *161*, 190–201. [CrossRef] [PubMed]
2. Ashmore, M. Assessing the future global impacts of ozone on vegetation. *Plant Cell Environ.* **2005**, *28*, 949–964. [CrossRef]
3. Sanderson, M.; Jones, C.; Collins, W.; Johnson, C.; Derwent, R. Effect of climate change on isoprene emissions and surface ozone levels. *Geophys. Res. Lett.* **2003**, *30*, 1936. [CrossRef]
4. Lu, X.; Hong, J.; Zhang, L.; Cooper, O.R.; Schultz, M.G.; Xu, X.; Wang, T.; Gao, M.; Zhao, Y.; Zhang, Y. Severe surface ozone pollution in China: A global perspective. *Environ. Sci. Technol. Lett.* **2018**, *5*, 487–494. [CrossRef]
5. Hu, C.; Kang, P.; Jaffe, D.A.; Li, C.; Zhang, X.; Wu, K.; Zhou, M. Understanding the impact of meteorology on ozone in 334 cities of China. *Atmos. Environ.* **2021**, *248*, 118221. [CrossRef]
6. Hoskins, B.J.; Rodwell, M.J. A model of the Asian summer monsoon. Part I: The global scale. *J. Atmos. Sci.* **1995**, *52*, 1329–1340. [CrossRef]
7. Rodwell, M.J.; Hoskins, B.J. Subtropical anticyclones and summer monsoons. *J. Clim.* **2001**, *14*, 3192–3211. [CrossRef]
8. Hou, X.; Zhu, B.; Fei, D.; Wang, D. The impacts of summer monsoons on the ozone budget of the atmospheric boundary layer of the Asia-Pacific region. *Sci. Total Environ.* **2015**, *502*, 641–649. [CrossRef]
9. Ma, J.; Lin, W.; Zheng, X.; Xu, X.; Li, Z.; Yang, L. Influence of air mass downward transport on the variability of surface ozone at Xianggelila Regional Atmosphere Background Station, southwest China. *Atmos. Chem. Phys.* **2014**, *14*, 5311–5325. [CrossRef]
10. Zhou, D.; Ding, A.; Mao, H.; Fu, C.; Wang, T.; Chan, L.; Ding, K.; Zhang, Y.; Liu, J.; Lu, A. Impacts of the East Asian monsoon on lower tropospheric ozone over coastal South China. *Environ. Res. Lett.* **2013**, *8*, 044011. [CrossRef]
11. Bian, J.; Yan, R.; Chen, H.; Lü, D.; Massie, S.T. Formation of the summertime ozone valley over the Tibetan Plateau: The Asian summer monsoon and air column variations. *Adv. Atmos. Sci.* **2011**, *28*, 1318–1325. [CrossRef]
12. Chen, T.-C.; Wang, S.-Y.; Huang, W.-R.; Yen, M.-C. Variation of the East Asian summer monsoon rainfall. *J. Clim.* **2004**, *17*, 744–762. [CrossRef]
13. Tong, M.; Zheng, Z.; Fu, Q. Evaluation of East Asian Meiyu from CMIP6/AMIP simulations. *Clim. Dyn.* **2022**, *59*, 2429–2444. [CrossRef]
14. Yihui, D.; Chan, J.C. The East Asian summer monsoon: An overview. *Meteorol. Atmos. Phys.* **2005**, *89*, 117–142. [CrossRef]
15. Zhang, R. Changes in East Asian summer monsoon and summer rainfall over eastern China during recent decades. *Sci. Bull.* **2015**, *60*, 1222–1224. [CrossRef]
16. Li, S.; Wang, T.; Huang, X.; Pu, X.; Li, M.; Chen, P.; Yang, X.Q.; Wang, M. Impact of East Asian summer monsoon on surface ozone pattern in China. *J. Geophys. Res. Atmos.* **2018**, *123*, 1401–1411. [CrossRef]
17. Vingarzan, R. A review of surface ozone background levels and trends. *Atmos. Environ.* **2004**, *38*, 3431–3442. [CrossRef]
18. Tanimoto, H.; Sawa, Y.; Matsueda, H.; Uno, I.; Ohara, T.; Yamaji, K.; Kurokawa, J.I.; Yonemura, S. Significant latitudinal gradient in the surface ozone spring maximum over East Asia. *Geophys. Res. Lett.* **2005**, *32*, 1–5. [CrossRef]
19. He, Y.; Uno, I.; Wang, Z.; Pochanart, P.; Li, J.; Akimoto, H. Significant impact of the East Asia monsoon on ozone seasonal behavior in the boundary layer of Eastern China and the west Pacific region. *Atmos. Chem. Phys.* **2008**, *8*, 7543–7555. [CrossRef]
20. Oltmans, S.J.; Levy, H. Seasonal cycle of surface ozone over the western North Atlantic. *Nature* **1992**, *358*, 392–394. [CrossRef]
21. Yin, C.; Solmon, F.; Deng, X.; Zou, Y.; Deng, T.; Wang, N.; Li, F.; Mai, B.; Liu, L. Geographical distribution of ozone seasonality over China. *Sci. Total Environ.* **2019**, *689*, 625–633. [CrossRef] [PubMed]
22. Liu, N.; Lin, W.; Ma, J.; Xu, W.; Xu, X. Seasonal variation in surface ozone and its regional characteristics at global atmosphere watch stations in China. *J. Environ. Sci.* **2019**, *77*, 291–302. [CrossRef] [PubMed]

23. Wang, Y.; Zhang, Y.; Hao, J.; Luo, M. Seasonal and spatial variability of surface ozone over China: Contributions from background and domestic pollution. *Atmos. Chem. Phys.* **2011**, *11*, 3511–3525. [CrossRef]
24. Hersbach, H.; Bell, B.; Berrisford, P.; Biavati, G.; Horányi, A.; Muñoz Sabater, J.; Nicolas, J.; Peubey, C.; Radu, R.; Rozum, I.; et al. ERA5 monthly averaged data on pressure levels from 1940 to present. *Copernic. Clim. Change Serv. Clim. Data Store* **2023**. [CrossRef]
25. O'Neill, B.C.; Tebaldi, C.; van Vuuren, D.P.; Eyring, V.; Friedlingstein, P.; Hurtt, G.; Knutti, R.; Kriegler, E.; Lamarque, J.F.; Lowe, J.; et al. The Scenario Model Intercomparison Project (ScenarioMIP) for CMIP6. *Geosci. Model Dev.* **2016**, *9*, 3461–3482. [CrossRef]
26. Meinshausen, M.; Nicholls, Z.R.J.; Lewis, J.; Gidden, M.J.; Vogel, E.; Freund, M.; Beyerle, U.; Gessner, C.; Nauels, A.; Bauer, N.; et al. The shared socio-economic pathway (SSP) greenhouse gas concentrations and their extensions to 2500. *Geosci. Model Dev.* **2020**, *13*, 3571–3605. [CrossRef]
27. Parrish, D.D.; Derwent, R.G.; Steinbrecht, W.; Stübi, R.; Van Malderen, R.; Steinbacher, M.; Trickl, T.; Ries, L.; Xu, X. Zonal similarity of long-term changes and seasonal cycles of baseline ozone at northern midlatitudes. *J. Geophys. Res. Atmos.* **2020**, *125*, e2019JD031908. [CrossRef]
28. VanderPlas, J.T. Understanding the lomb–scargle periodogram. *Astrophys. J. Suppl. Ser.* **2018**, *236*, 16. [CrossRef]
29. Springford, A.; Eadie, G.M.; Thomson, D.J. Improving the Lomb–Scargle Periodogram with the Thomson Multitaper. *Astron. J.* **2020**, *159*, 205. [CrossRef]
30. Zechmeister, M.; Kürster, M. The generalised Lomb-Scargle periodogram-a new formalism for the floating-mean and Keplerian periodograms. *Astron. Astrophys.* **2009**, *496*, 577–584. [CrossRef]
31. Li, J.; Zeng, Q. A unified monsoon index. *Geophys. Res. Lett.* **2002**, *29*, 115. [CrossRef]
32. Zhisheng, A.; Guoxiong, W.; Jianping, L.; Youbin, S.; Yimin, L.; Weijian, Z.; Yanjun, C.; Anmin, D.; Li, L.; Jiangyu, M. Global monsoon dynamics and climate change. *Annu. Rev. Earth Planet. Sci.* **2015**, *43*, 29–77. [CrossRef]
33. Ding, R.; Ha, K.-J.; Li, J. Interdecadal shift in the relationship between the East Asian summer monsoon and the tropical Indian Ocean. *Clim. Dyn.* **2010**, *34*, 1059–1071. [CrossRef]
34. Zhao, G.; Huang, G.; Wu, R.; Tao, W.; Gong, H.; Qu, X.; Hu, K. A new upper-level circulation index for the East Asian summer monsoon variability. *J. Clim.* **2015**, *28*, 9977–9996. [CrossRef]
35. Wang, Y.; Shen, J.; Wang, H.; Wu, G.; Chen, Y.; Liu, T.; Gong, D.; Ou, J.; Shi, Y.; Zhang, T. Unexpected seasonal variations and high levels of ozone observed at the summit of Nanling Mountains: Impact of Asian monsoon on southern China. *Atmos. Environ.* **2021**, *253*, 118378. [CrossRef]
36. Ma, M.; Gao, Y.; Wang, Y.; Zhang, S.; Leung, L.R.; Liu, C.; Wang, S.; Zhao, B.; Chang, X.; Su, H.; et al. Substantial ozone enhancement over the North China Plain from increased biogenic emissions due to heat waves and land cover in summer 2017. *Atmos. Chem. Phys.* **2019**, *19*, 12195–12207. [CrossRef]
37. Ding, Y.; Liang, P.; Liu, Y.; Zhang, Y. Multiscale variability of Meiyu and its prediction: A new review. *J. Geophys. Res. Atmos.* **2020**, *125*, e2019JD031496. [CrossRef]
38. Sampe, T.; Xie, S.-P. Large-scale dynamics of the meiyu-baiu rainband: Environmental forcing by the westerly jet. *J. Climate* **2010**, *23*, 113–134. [CrossRef]
39. Ding, A.J.; Fu, C.B.; Yang, X.Q.; Sun, J.N.; Zheng, L.F.; Xie, Y.N.; Herrmann, E.; Nie, W.; Petäjä, T.; Kerminen, V.M.; et al. Ozone and fine particle in the western Yangtze River Delta: An overview of 1 yr data at the SORPES station. *Atmos. Chem. Phys.* **2013**, *13*, 5813–5830. [CrossRef]
40. Qian, J.; Liao, H.; Yang, Y.; Li, K.; Chen, L.; Zhu, J. Meteorological influences on daily variation and trend of summertime surface ozone over years of 2015–2020: Quantification for cities in the Yangtze River Delta. *Sci. Total Environ.* **2022**, *834*, 155107. [CrossRef]
41. Liu, Z.; Wang, Y.; Gu, D.; Zhao, C.; Huey, L.G.; Stickel, R.; Liao, J.; Shao, M.; Zhu, T.; Zeng, L.; et al. Summertime photochemistry during CAREBeijing-2007: RO_x budgets and O_3 formation. *Atmos. Chem. Phys.* **2012**, *12*, 7737–7752. [CrossRef]
42. Yang, Y.; Liao, H.; Li, J. Impacts of the East Asian summer monsoon on interannual variations of summertime surface-layer ozone concentrations over China. *Atmos. Chem. Phys.* **2014**, *14*, 6867–6879. [CrossRef]
43. Chen, F.; Chen, J.; Huang, W. Weakened East Asian summer monsoon triggers increased precipitation in Northwest China. *Sci. China Earth Sci.* **2021**, *64*, 835–837. [CrossRef]
44. Cherchi, A.; Fogli, P.G.; Lovato, T.; Peano, D.; Iovino, D.; Gualdi, S.; Masina, S.; Scoccimarro, E.; Materia, S.; Bellucci, A.; et al. Global Mean Climate and Main Patterns of Variability in the CMCC-CM2 Coupled Model. *J. Adv. Model. Earth Syst.* **2019**, *11*, 185–209. [CrossRef]
45. Moon, S.; Ha, K.-J. Future changes in monsoon duration and precipitation using CMIP6. *Npj Clim. Atmos. Sci.* **2020**, *3*, 45. [CrossRef]